JOURNAL OF CATALYSIS 140, 209–225 (1993)

The Chemical State of Gallium in Working Alkane Dehydrocyclodimerization Catalysts. *In Situ* Gallium *K*-Edge X-ray Absorption Spectroscopy

GEORGE D. MEITZNER, ENRIQUE IGLESIA, JOSEPH E. BAUMGARTNER, AND ENOCH S. HUANG[1]

Corporate Research Laboratories, Exxon Research and Engineering Company, Route 22 East, Annandale, New Jersey 08809

Received May 1, 1992; revised November 3, 1992

Ga species in H-ZSM5 zeolites catalyze rate-limiting dehydrogenation steps during the conversion of alkanes to aromatics. Specifically, they promote the recombinative desorption of H-adatoms as H_2 and thus inhibit undesired cracking reactions. Here, we describe studies of the physical and chemical state of Ga using *in-situ* X-ray absorption at the Ga *K*-edge. Ga^{+3} species initially present in fresh catalysts reduce at temperatures below 770 K during hydrogen pretreatment or propane reactions. Reduced Ga is present in highly dispersed form without Ga nearest neighbors, probably as a monomeric hydride species coordinated to basic oxygens within zeolite channels. These hydride species are driven to release molecular hydrogen by the high surface hydrogen fugacities that develop during propane dehydrocyclodimerization on H-ZSM5. Reduced Ga species reoxidize to Ga^{+3} when samples are cooled to room temperature in flowing H_2, suggesting that active forms of Ga exist only at reaction conditions. This work illustrates the critical need for *in-situ* techniques to establish the chemical form of catalytic sites and the misleading conclusions that can arise from the exclusive use of pre- and postreaction characterization to suggest the nature of the catatlytic sites.

INTRODUCTION

Ga (*1–4*) and Zn (*5*) promote the reactions of alkanes on metal oxides and specifically the formation of aromatic molecules via sequential dehydrogenation, oligomerization, and cyclization steps. These types of materials are presently used in the CYCLAR process for conversion of light alkanes to aromatics (*4*). Recent reports (*6–12*) have provided increasing support for an earlier proposal that Zn (*5*) and Te (*13*) species within zeolite channels catalyze the rate-limiting removal of H-adatoms as H_2 from zeolite surfaces. These recombinative desorption steps lower the high hydrogen surface fugacities that slow down dehydrogenation steps and lead to cracking reactions as the predominant hydrogen removal pathway during alkane reactions on H-ZSM5 (*10–12*).

The chemistry of the active Ga species in these materials, and the means by which they catalyze hydrogen removal as H_2, are poorly understood. The role of Ga ions as a Lewis acid that stabilizes hydride species required for H^+–H^- recombination was recently proposed without direct experimental evidence (*6, 10–12*). This behavior of Ga species is particularly interesting because Ga is not a good hydrogenation catalyst and in fact not a commonly used catalytic element; yet, Ga ions on acid supports (e.g., H-ZSM5) promote dehydrogenation steps more effectively than better dehydrogenation catalysts (e.g., Pt). The low concentrations of Ga (1–2 wt%) in these materials preclude the use of X-ray diffraction for their structural characterization. Solid-state

[1] Current address: Department of Chemistry, Princeton University, Princeton, NJ 08544.

0021-9517/93 $5.00

NMR (*14, 15*) and extended X-ray absorption fine structure (EXAFS) (*16*) were previously used in the study of gallosilicate microporous materials, which are inactive in propane aromatization reactions and where all Ga species are initially present within the zeolite framework. To our knowledge, structural techniques have not been previously applied to the study of actual catalysts containing extraframework Ga under catalytic reaction conditions.

EXPERIMENTAL

The chemical state of Ga in working catalysts was characterized by Ga *K*-edge X-ray absorption spectroscopy (XAS) using beamline X10C at the National Synchrotron Light Source, Brookhaven National Laboratory. The beamline setup has been described in detail elsewhere (*17*); it includes a Si(220) two-crystal monochromator, and a bent cylindrical mirror in order to focus and to reject higher energy harmonics. The resolution of the monochromator at the Ga *K*-edge (10,368 eV) was 4 eV. Spectra were obtained with a 0.5 eV increment between data points near the absorption edge and an increment of 0.02 $Å^{-1}$ (wavenumbers) in the extended X-ray absorption fine structure (EXAFS) region. Ga *K*-edges were fitted by linear combinations of spectra from standard Ga^{+3} compounds and from Ga metal. The resulting best fit gave the fraction of the Ga present in various reduced and oxidized states (*18*). $Ga(NO_3)_3$ hydrate (Johnson Matthey) and a gallosilicate sample with ZSM5-type structure and containing 0.5% Ga in the framework structure (*19*) were used as standards for octahedral and tetrahedral Ga^{+3} species, respectively. Ga metal granules (Aldrich, 99.9999%) were used as the zero-valent Ga standard.

Ga/H-ZSM5 materials were prepared by impregnation of H-ZSM5 (Zeochem, Si/Al = 14.5) with a Ga nitrate solution. These samples were calcined in air at 623 K for 2h and pretreated in H_2 or propane *in situ* during XAS and catalytic experiments. Catalytic tests were performed in the *in-situ* XAS cell (*20*) and in a gradientless batch reactor (*13*). The products were analyzed by gas chromatography and mass spectrometry.

X-ray absorption spectra were measured on a Ga/H-ZSM5 wafer formed by pressing 1 g of the material at 35 MPa in a stainless steel die (3.3 cm diameter). The *in-situ* XAS cell was essentially the same as one described previously (*20*). The wafer was held within the cell by a circular mount that also provided the resistive heating required to reach reaction temperatures. This mount, through which He, H_2, and propane could flow, was located between aluminized Kapton windows. The cylindrical cell was gastight; still, it was contained within an aluminum box with Kapton windows, which was flushed continuously with He in order to exclude oxygen from the sample even in case of a leak in the primary cell vessel. Hydrogen (Matheson, 99.99%) was purified by a catalytic Pd bed and by a 13X molecular sieve. He (Matheson, 99.999%) and propane (Air Products, >99.5%) were dried by also flowing through a 13X molecular sieve. All gases arrived at the *in-situ* XAS cell through welded tubing in order to minimize contamination by leakage through connecting joints.

NEAR-EDGE AND EXAFS DATA ANALYSIS AND RESULTS

The X-ray absorption spectrum of a calcined Ga (2.0 wt%)/H-ZSM5 catalyst is shown in Fig. 1. The sharp increase in absorbance at 10368 eV defines the Ga *K*-edge and results from the excitation of Ga 1*s* electrons by incoming X-ray photons. As the X-ray energy approaches the binding energy of 1*s* electrons, resonant excitations to vacant bound states with *p*-type symmetry become possible. These orbitals are often hybridized and involved in bonding; consequently, the resulting *K*-edge structure is very sensitive to the chemical environment and to the bonding symmetry of the absorber atoms (*18*). Also, the 1*s* binding energy, which defines the *K* absorption edge,

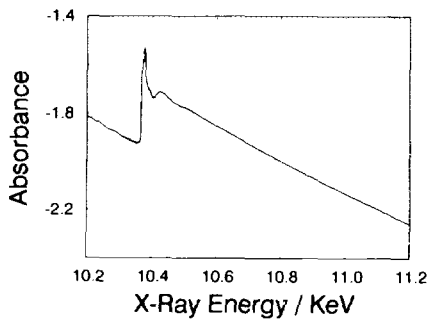

FIG. 1. X-Ray absorption spectrum at the K-edge of Ga in the calcined 2.0% wt. Ga/H-ZSM5 as received (room temperature). The sharp increase in absorbance near 10.4 keV is the edge. The near edge region extends about 50 eV above the edge. The EXAFS, when present, occurs as series of oscillations in absorbance up to 1 keV above the edge.

is influenced strongly by the oxidation state of the absorber; the edge shifts to higher energy as oxidation occurs (*21*).

The energy region slightly above the absorption edge ($\Delta E = +50$ eV) reflects the absorption of X rays that excite 1*s* electrons into the continuum of (unbound) states above the vacuum level. Scattering interactions of the ejected electrons with atoms near the absorber lead to oscillations in the absorption coefficients and to fine structure in this extended absorption region. The resulting EXAFS spectrum $[X(K)]$ is described by

$$\chi(K) = \sum \frac{N_j}{KR_j^2} \cdot F(K) \exp(-2K^2\sigma_j^2) \cdot \sin(2KR_j + 2\delta(K)) \quad (1)$$

$$K = [2m(E - E_0)]^{1/2}/\hbar. \quad (2)$$

E and E_0 are the incident photon energy and the core electron binding energy, respectively, m is the mass of the electron, and $\hbar$ is Planck's constant divided by 2π. N_j is the number of neighboring atoms in the jth shell located a distance R_j away from the absorber, and σ_j^2 is the Debye–Waller factor (the mean-square relative displacement of these neighbors about R_j, arising from thermal motion or structural disorder). The $F(K)$ and $2\delta(K)$ are the element-specific scattering factor and phase-shift function, respectively. The summation of these terms in Eq. (1) occurs over all coordination shells at distances R_j.

K-edge and EXAFS data were analyzed by fixing the zero point in the energy scale at the first inflection point in the edge region. The pre-edge part of the spectrum (50 to 20 eV below the edge) was then fit by a straight line. A cubic spline polynomial with three equally spaced knots was used to describe the high energy side of the edge (10 to 750 eV above the edge). Both fitting functions were extrapolated to the absorption threshold energy and the entire spectrum was normalized by the height of the resulting absorbance step at the edge. The near-edge and EXAFS spectra were obtained by subtracting the pre-edge and post-edge fitting function from the raw absorption spectrum. Representative edge spectra for several Ga/H-ZSM5 samples are shown in Fig. 2.

The energy scale was then converted to K units (wavenumbers, $Å^{-1}$) and the EXAFS data (weighted by K^1) was subjected to a

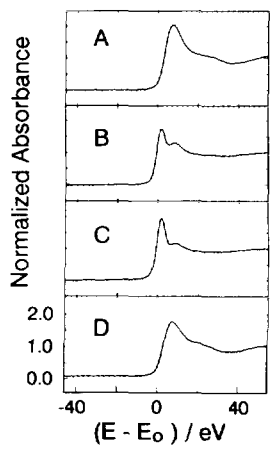

FIG. 2. Near-edge spectra of Ga/H-ZSM5: (a) at the beginning of the hydrogen treatment at 780 K; (b) at an intermediate state of reduction; (c) after 6–8 h in hydrogen at 780 K (steady-state); (d) treatment as in (c) but cooled to RT before obtaining spectra.

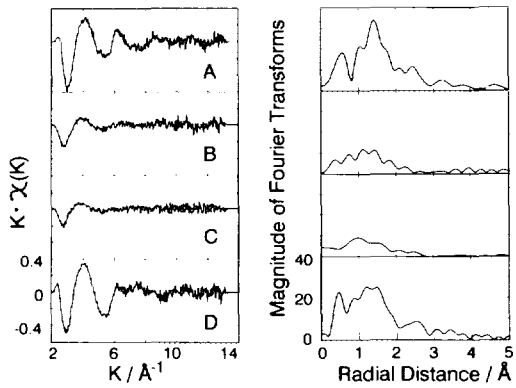

FIG. 3. K-weighted EXAFS [$K * \chi(K)$] and Fourier-transformed EXAFS (radial structure functions) of Ga/H-ZSM5: (a) at the beginning of the hydrogen treatment at 780 K; (b) at an intermediate state of reduction; (c) after 6–8 h in hydrogen at 780 K (steady-state); (d) treatment as in (c) but then cooled in flowing H_2 to RT before obtaining spectra.

Fourier transform in the range from 2 to 13 $Å^{-1}$. Raw EXAFS data [$K * \chi(K)$] and the magnitudes of the corresponding Fourier transforms (radial structure functions, RSF) are shown for several Ga/H-ZSM5 samples in Fig. 3. During reduction at high temperature, the EXAFS almost disappeared, but appeared again in slightly modified form, when the reduced samples were cooled to room temeprature (RT) in flowing hydrogen.

Our analysis of the EXAFS data was limited to a comparison of the magnitudes of the peak located at 1.4 Å in the Ga radial structure function (Fig. 3). The remaining EXAFS features in the samples reduced at high temperature were so weak that distinguishing neighboring atoms as either Ga or oxygen was difficult. In general, the electron scattering factor ($F(K)$ in Eq. (1)) decays much faster when absorber atoms are bound to lighter elements (*22*). The rapid damping of the $K \cdot F(K)$ function in K-space (Fig. 3a) suggests that Ga atoms were predominantly bonded to oxygen (or carbon) at all experimental conditions.

Several Ga compounds of known crystal structure were used as standards to identify Ga species formed on Ga/H-ZSM5 during pretreatment and catalysis. The spectrum of $Ga(NO_3)_3 \cdot xH_2O$ ($x \approx 6$) (Johnson Matthey), the Ga salt used in catalyst preparation, was measured from a wafer consisting of 1 g of silica (Davidson 12) and 0.2 g of Ga nitrate. The crystal structure of Ga nitrate has not been determined as far as we know. However, we believe the K-edge of the gallium in this compound is representative of gallium in an octahedral environment. First, aqueous Ga^{3+} ions show octahedral coordination by aquo ligands (*23*). Second, Al^{3+} ions in $Al(NO_3)_3 \cdot xH_2O$ (x = 6, 8, or 9) also have octahedral coordination by aquo ligands (*24*), and most gallium and aluminum compounds are isostructural. Finally, we also found that equal contributions of our tetrahedral (framework) gallium standard spectrum and the Ga nitrate spectrum accurately describe the Ga edge spectrum from β-Ga_2O_3, in which Ga^{3+} ions are equally distributed between tetrahedral and octahedral sites. Also, the EXAFS analysis shows that Ga^{3+} ions in the nitrate have six oxygen neighbors in their first coordination sphere, consistent with octahedral Ga coordination.

The XAS spectrum of tetrahedral Ga species was obtained from a ZSM5 sample synthesized with 0.5% Ga in the framework using a 1-g wafer of the pure gallosilicate material (*19*). Tetrahedral framework Ga species were stable even after extensive reduction in hydrogen at 780 K; these gallosilicate materials were inactive in propane aromatization reactions below 800 K; they became active only after extensive removal of Ga from the framework by calcination treatments above 800 K. A Ga metal standard was prepared by mixing 0.1 g of the metal with 0.9 g silica in a grinding mill.

A final standard spectrum was obtained by reduction of the Ga/H-ZSM5 catalysts at 780 K in hydrogen for 10 h; after this treatment, subsequent spectra were unaffected by longer reduction times. This spectrum reflects a steady-state catalytic material and is denoted GaH_x, for reasons that

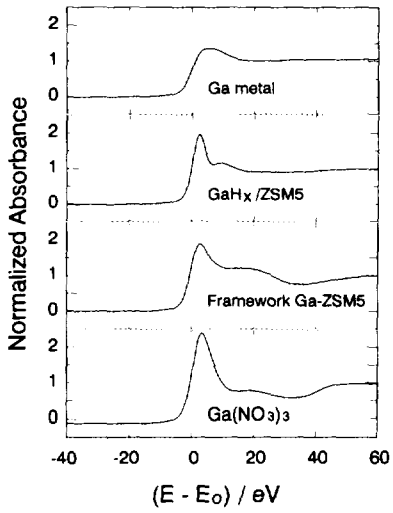

FIG. 4. Near-edge XAS spectra of four Ga standards. Sample denoted as GaH_x is the same as the steady-state sample shown as part c in Figs. 2, 3, 6, 7, and 8.

we discuss later. The XAS spectra of all standard materials are shown in Fig. 4. All spectra, except for the GaH_x spectrum, were obtianed at RT without further pretreatment. The GaH_x spectrum was obtained at 780 K after pretreatment in H_2 for 10 h. Spectra were also taken of the GaH_x sample after cooling in H_2 to RT.

We used near-edge spectra from our standard materials to analyze sample spectra obtained across a wide range of temperatures. Among our standards, the GaH_x near-edge spectrum was measured at high temperature where the species is stable. Gallium nitrate thermally decomposes to Ga_2O_3 at 470–530 K (*26*); therefore, we have used a low-temperature spectrum from the nitrate throughout this work. We have confirmed that the spectrum from the tetrahedral gallium standard (framework Ga in ZSM5) was not affected by extended reduction in H_2 at 780 K. We did not measure the high-temperature spectrum of Ga metal because Ga metal melts near room temperature.

In another series of experiments, catalysts previously subjected to two reduction (773 K)/oxidation (623 K) cycles were exposed to propane (20 kPa) at 623 K with He as the carrier gas and the temperature increased to 800 K. Spectra were measured at 800 K while flowing the propane/He reactant mixture. A residue left in the *in-situ* XAS cell after about 5 h contained aromatic compounds ranging from toluene to polynuclear aromatics, but apparently no Ga compounds.

GALLIUM SPECIES DURING REDUCTION AND PROPANE REACTIONS

Changes in the Ga oxidation state and structure during hydrogen pretreatment and catalytic reactions of propane clearly shift the energy of the absorption edge, modify the shape of the near-edge region, and decrease the intensity of the fine structure oscillations in the EXAFS region. The absorption energy shifts were accurately determined by comparing the edge energy with that of a germanium foil (11,103 eV *K*-edge) placed between two detectors after the catalyst sample. The edge energies measured for all standard Ga samples are listed in Table 1.

We established structural and chemical changes during the course of the Ga^{+3} reduction by describing the experimental X-ray absorption spectra on Ga/H-ZSM5 samples as linear combinations of weighted spectra of standard Ga samples (Fig. 4) (*18*).

TABLE 1

Absolute Energies of Ga *K* Absorption Edges for Standards Used in This Work

Standard	Edge energy (eV)	ΔE (eV)
Ga metal	10367.1 eV	0
GaH_x	10368.0	0.9
Tetrahedral Ga^{3+}	10372.7	5.6
Octahedral Ga^{3+}	10373.3	6.2

Note. The positions of the edges are defined by the first inflection points. The absolute positions were determined by reference to the *K*-edge measured simultaneously from a Ge foil (11,103 eV) placed between two detectors after the catalyst sample.

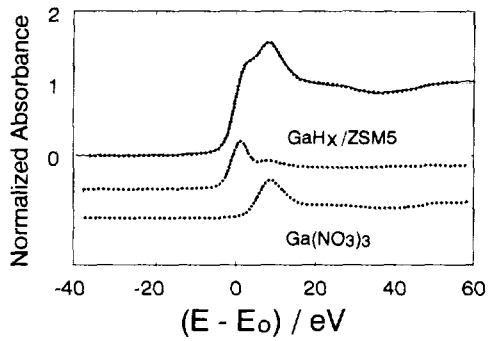

FIG. 5. Near-edge spectrum of Ga/H-ZSM5 sample after 2.5 h reduction in hydrogen at 780 K (solid line) and the calculated spectrum (dotted line) using spectra from the four standards. The contributions from GaH_x and $Ga(NO_3)_3 \cdot x\,H_2O$ are also shown. The correspondence shown by the upper curved is typical of the qualities of all the edge fits.

Absorption edge spectra from calcined, partly reduced, and fully reduced Ga/H-ZSM5 samples are shown in Fig. 2. A typical fit for the edge spectra of a partially reduced sample is shown in Fig. 5, where the contributions from the GaH_X and the octahedral Ga nitrate standards are also shown. The best fit is shown as a dotted line in the top spectrum of Fig. 5; it also included contributions from tetrahedral and metallic Ga standards, which are not shown. All Ga states observed in Ga/H-ZSM5 catalysts were described accurately by linear combinations of the four standard materials used in our study: tetrahedral Ga^{+3}, octahedral Ga^{+3}, Ga metal, and the steady-state GaH_x catalyst.

We have also used the EXAFS data from Ga/H-ZSM5, even though the information contained in the fine structure data was limited. The corresponding EXAFS and radial structure functions for the edge spectra in Fig. 2 are shown in Fig. 3. The Ga EXAFS intensity gradually decreased and the features in the fine structure almost disappeared completely during the reduction. The intensity of such features was insufficient to support much quantitative analysis. We measured, however, the intensity of the 1.42-Å peak (uncorrected for phase-shift) in order to monitor changes in the Ga chemical environment during reduction and propane reactions.

THE REDUCTION OF GALLIUM SPECIES IN Ga/H-ZSM5

The reduction of Ga_2O_3 to Ga_2O occurs in vacuum at about 773 K (*26*) and the reduction to Ga metal is favored by thermodynamics at 780 K for $[H_2O]/[H_2]$ ratios less than 10^{-5}, conditions clearly achievable during H_2 pretreatment and propane reactions (*25*). Ga spectra in Ga/H-ZSM5 underwent significant changes during hydrogen treatment or propane reactions at 780 K; these changes, however, were reversed by cooling the samples in hydrogen to RT. Figure 6 shows energy shifts in the Ga *K*-absorption edge during hydrogen reduction and subsequent cooling. The absorption edge corresponding to Ga_2O_3 was slowly replaced during reduction by one resembling that of the steady-state reduced samples (GaH_x). This edge appeared several electron volts below the oxidized sample edge and increased in intensity as the original Ga^{+3} absorption edge features decreased in intensity. The contributions of one of the oxidized and one of the reduced components in the spectrum for a Ga/H-ZSM5 sample at an intermediate state of reduction are shown in Fig. 5.

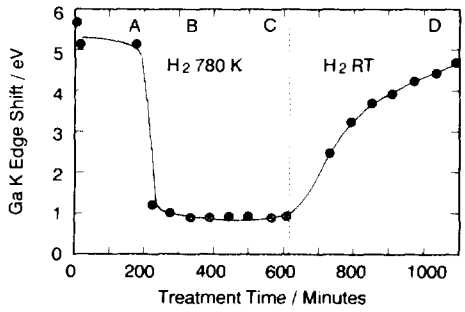

FIG. 6. Gallium *K*-edge energy shifts during reduction in H_2 at 780 K and during cooling to RT in flowing H_2.

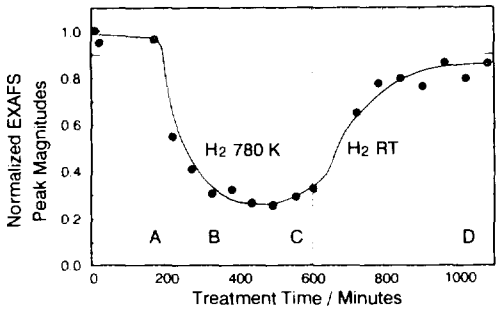

FIG. 7. Normalized magnitudes of the 1.42 Å (uncorrected) peak in the radial structure functions during reduction (H_2, 780 K) and subsequent cooling (H_2, RT) of Ga/H-ZSM5.

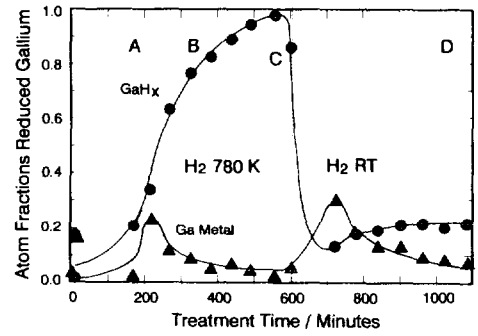

FIG. 9. Atomic fraction of Ga present as Ga metal (▲) and as GaH_x (●) during reduction (H_2, 780 K) and subsequent cooling (H_2, RT) of Ga/H-ZSM5. The shape of the Ga metal curve suggests that Ga metal is formed as an intermediate species and ultimately converted to the steady-state GaH_x form.

The deconvolution of these spectra into contributions from standard forms of Ga are shown in Figs. 8 and 9. The Ga in the calcined starting material was present as Ga^{+3} equally distributed between octahedral and tetrahedral sites (Fig. 8), as expected for bulk Ga_2O_3. As the reduction proceeds, some metallic Ga forms and then disappears (Fig. 9); Ga metal appears to act as a precursor to the final steady-state form of Ga, which we have described as GaH_x. These changes and the ultimate formation of this steady-state GaH_x form initially required several hours in flowing hydrogen at 780 K.

The intensity of the single strong peak in the EXAFS spectrum (Fig. 3) decreases with increasing reduction time (Fig. 7). It is well known that thermal motions of atoms weaken the fine structure of X-ray absorption spectra as materials approach their melting point (*33*). The effect is represented by the Debye–Waller factor (σ_j^2) in Eq. (1). The EXAFS of elements in refractory oxide compounds, such as oxygen in Al_2O_3, is influenced by thermal motion only at very high temperatures; in contrast, such effects are observed in metallic phases at much lower temperatures. Ga metal melts near RT (302 K); consequently, it is unlikely to show any EXAFS features at 780 K. Thus, one possible explanation for the decline in EXAFS intensity as reduction proceeds is the formation of metallic Ga. It would not contribute to the EXAFS features in the spectrum whether or not it is atomically dispersed or not.

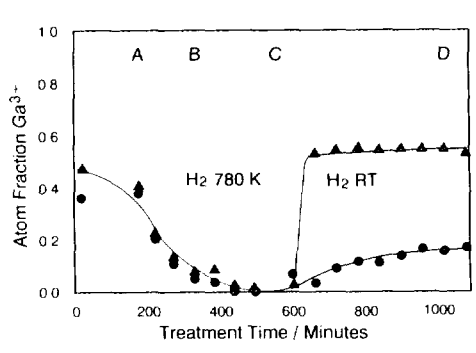

FIG. 8. Atomic fraction of Ga present as Ga^{+3} tetrahedral (▲) or octahedral (●) during reduction (H_2, 780 K) and subsequent cooling (H_2, RT) of Ga/H-ZSM5.

We do not believe that the formation of liquid Ga metal explains the disappearance of EXAFS features during reduction. The absorption edge of the steady-state reduced Ga/H-ZSM5 sample does not resemble that of Ga metal (cf. Figs. 4 and 5). Also, the EXAFS amplitude reached a minimum, but did not disappear, at an interatomic distance consistent with coordination of Ga to oxygen atoms. Finally, molten Ga metal would have sintered, and probably left the zeolite

channels, because extremely strong interatomic forces between Ga atoms would favor Ga–Ga interactions (Ga melts at 302 K but boils above 2200 K) over monomeric reduced Ga species. The resulting sintered Ga aggregates would not reoxidize readily when the sample is cooled and would be recognizable at RT by the edge and EXAFS spectra characteristic of solid Ga metal. We propose instead that the steady-state Ga/H-ZSM5 spectra correspond to Ga hydride monomeric species (GaH_x) that would be expected to coordinate to one or more basic framework oxygen within zeolite channels without full oxidation to Ga^{+3} ions.

Ga and H electronegativities are very similar; therefore, Ga–H bonds in GaH_x species are covalent in nature and available electrons are equally shared between the two atoms. As we observe, reactions between Ga cations and hydride (H^-) species should lead to net reduction of the former because of significant transfer of electron density from H^- to the electropositive cations. The resulting valency of Ga atoms in reduced catalysts is between 0 and 1; it cannot be determined more precisely by our XAS measurements.

Recent reports suggest that the reduction of Ga^{+3} in Ga_2O_3/H-ZSM5 mixtures is influenced by the intimacy of mixing between the two components (*34*). In our studies, the initial reduction of Ga^{+3} species was slow compared with subsequent reductions (e.g., Fig. 10). This also suggested that migration of Ga^{+3} species, initially present as Ga_2O_3 on the outer zeolite surface, to intracrystalline sites precedes their reduction to GaH_x species. The initial reduction appears to be limited by the diffusion of $Ga^{+\delta}$ intermediates, possibly Ga^{+1} as mobile Ga_2O compounds. Subsequent reductions, which no longer required macroscopic mobility, occurred significantly faster.

These GaH_x species reoxidized to Ga^{+3} upon cooling to RT in flowing hydrogen, as shown by the shift in its *K*-edge, by its chemical state determined from *K*-edge analysis using standard Ga compounds, and by the higher intensity of its EXAFS features. This oxidation at RT and the subsequent reduction with hydrogen or propane at 780 K was reversible and was replicated several times. Ga metal would scavenge oxygen very effectively if O_2 were present in the cell as an impurity; however, it would have required 100-ppm oxygen levels in the hydrogen stream and about 20 h to reoxidize all the Ga in our sample. Hydrogen (initially 99.99%) was purified to reduce its O_2 and H_2O content below 1 ppm before entering the sample cell. Therefore, oxygen or water impurities in the hydrogen feed can not be responsible for this oxidation, which occurs in less than 2 h at RT. There are, however, oxidizing species always present on H-ZSM5 channel surfaces. These include protons formed during the Ga^{+3} reduction and located at bridging hydroxyl and silanol groups. Metal clusters within Y-zeolite channels can undergo oxidation by reactions with protons formed during the initial reduction of exchanged metal cations (*35*). This oxidation occurs during heating of reduced catalysts even in inert atmospheres.

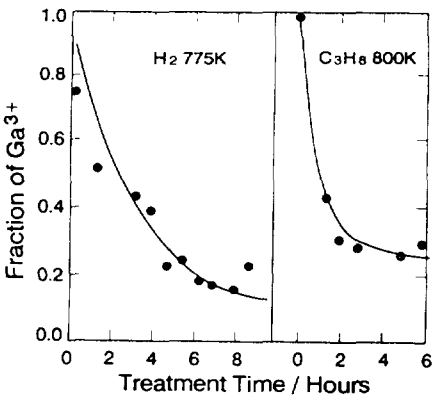

FIG. 10. Atomic fraction of Ga present in unreduced Ga^{+3} species during: (a) reduction in H_2 at 775 K; (b) propane reaction (20 kPa, 800 K) after two reduction (775 K)–oxidation (623 K) cycles.

Clearly, the initial equimolar distribution of Ga^{+3} ions between tetrahedral and octahedral sites, characteristic of Ga_2O_3, is not restored by the oxidation of GaH_x within H-ZSM5 channels near room temperature (Fig. 8). Instead, Ga^{+3} ions show predominant tetrahedral symmetry, consistent with

their preferential location in "epitaxial" positions as extraframework species with structures resembling those of framework Al^{+3} ions within the ZSM5 framework. The rapid rereduction of these species suggests that tetrahedral Ga^{+3} species do not reside within the ZSM5 framework. Tetrahedral Ga^{+3} within our gallosilicate structures reduced very slowly in hydrogen even above 873 K.

Reactions of propane on calcined Ga/H-ZSM5 samples at 780–800 K also reduce Ga^{+3} species to GaH_x (Fig. 10). Changes in X-ray absorption spectra during reaction resembled those observed during hydrogen pretreatment. During separate experiments in a catalytic reactor, the propane conversion rate and aromatics selectivity increased with reaction time when calcined Ga/H-ZSM5 samples were not prereduced before propane reactions (Table 2). Reduction of Ga/H-ZSM5 to its active form during propane reactions is consistent with the generation of high surface hydrogen fugacities on H-ZSM5 surfaces during catalysis (*10, 11*). These high surface fugacities arise from the rate-limiting nature of the hydrogen removal steps and lead to hydrocracking of C–C bonds in hydrocarbons. Not surprisingly, they also appear to lead to the hydrogenolysis of Ga–O bonds and to the reduction of Ga^{+3} in unreduced Ga/H-ZSM5 during catalytic reactions of light alkanes.

We suggest that the steady-state product of the reduction of Ga^{+3} species in either hydrogen or propane at 780–800 K is a hydride form of Ga stabilized by interactions with basic oxygens within ZSM5 channels. These species may represent zeolite-analogs of $GaHCl_2$ (*26*) or $R_3N \cdot GaH_3$ (*38*), which are relatively stable Ga hydride compounds compared to GaH_3. The trialkylamine gallane adduct is known from its X-ray diffraction pattern to be monomeric (*38*). In H-ZSM5, basic oxygen sites within zeolite channels would replace Cl or trialkylamine as the basic ligand required to stabilize monomeric GaH_x species.

Coordination of partially reduced Ga species (Ga_2O) to framework oxygen in H-ZSM5 was previously proposed to explain temperature-programmed reduction profiles of Ga/H-ZSM5 materials (*34*). Mixtures of Ga_2O_3 and H-ZSM5 reduced at lower temperatures than Ga_2O_3, but these effects were sensitive to the number of acidic protons in H-ZSM5 (*34*). This proposal is consistent with our EXAFS results, which show that the coordination number of Ga with oxygen nearest neighbors decreases from near six (octahedral Ga^{+3}) to about one. This proposal also accounts for the reduction–oxidation behaviour of these ions.

Our measurements of dihydrogen consumption during reduction of calcined Ga/H-ZSM5 samples confirm that Ga^{+3} (in Ga_2O_3) reduces only to Ga^{+1} even after 2–6 h at 773 K in (4%) H_2/Ar mixtures. In contrast, Ga_2O_3 on Al_2O_3 samples reduce completely to Ga^0 during the same treatment. Calcined Ga/H-ZSM5 consume 1.8 mol of H_2 per Ga g-atom, consistent with a valence reduction from Ga^{+3} to Ga^{+1} (*41*). Our near edge measurements show the complete absence of Ga^{+3} in reduced samples; thus, the observed Ga^{+1} valence in reduced samples is unlikely to arise from mixtures of Ga^0 and Ga^{+3}. We conclude that reduction treatments lead to Ga^{+1} species at cation exchange sites, where strong interactions with framework oxygen stabilize these species against further reduction to Ga^0.

This interaction between Ga and basic framework oxygens occurs without significant oxidation of Ga ions in the presence of H-adatoms, as evidenced by the similarities in *K*-edge energy between our samples and Ga metal, because hydrogen atoms can act as both reduction and oxidation agents and some hydrides of Ga indeed decompose as they cool (*26*). Such Ga hydride species would form at steady state during hydrogen treatment or propane catalysis at 780–800 K because the decomposing hydride species is continuously replenished by dihydrogen or by hydrogen adatoms dissociated from propane during reaction. Both dihydrogen dissociation and propane conversion rates become very slow at low temperatures and

TABLE 2

Catalytic and X-ray Absorption Data on H-ZSM5 and Ga/H-ZSM5

Ga content (% wt.) propane reactions[a]	H-ZSM5				
	0	0.3 (reduced)	2.0 (calcined)[e]	2.0 (activated during reaction)[f]	2.0 (reduced, 2h)
Aromatics turnover turnover rate (per Al-atom, 10^{-3} s^{-1})	0.34	0.49	1.2	4.6	3.91
(Aromatization/ cracking) ratio	0.042	0.16	0.61	1.37	1.05
Hydrogen removed as H_2 (%)[c]	4.0	7.5	19.6	28.1	23
2-Methyl-2-pentene reactions[b]					
4-Methyl-2-pentene rate (10^3 · molec · Al^{-1} · s^{-1})	5.6	—	7.00	—	5.20
3-Methyl-2-pentene rate (10^3 · (molec · Al^{-1} · s^{-1})	1.67	—	2.38	—	1.51
Acid strength ratio[g]	0.30	—	0.34	—	0.29
X-ray absorption[d]					
Reduced Ga content (% wt)	0	0.12	0.35	1.4	1.4
NH_3 adsorption[h]	0.82	—	0.77	—	0.62
Strongly adsorbed NH_3 (NH_3/Al)					

[a] 773 K, 26.6 kPa propane, balance He, 7.2–11.2% conversion.
[b] 448 K, 0.083 h on stream, 7 kPa 2-methyl-2-pentene, 34.3–38.1% conversion.
[c] Percentage of hydrogen in reacted propane that appears as H_2.
[d] From deconvolution of near-edge data; GaH_x component.
[e] 0.67 h time on stream, not prereduced before catalytic measurements.
[f] 7.0 h time on stream, not prereduced before catalytic measurements.
[g] (3-Methyl-2-pentene/4-methyl-2-pentene).
[h] RT adsorption, strong adsorption defined as that requiring temperatures above 573 K for desorption.

can no longer restore the decomposing hydride, which becomes less favored by thermodynamics at lower temperatures (*25*). The resulting unsaturated Ga–O species acquire a stable structure (predominantly tetrahedral, Fig. 8) by reconstructing bonds with neighboring oxygen atoms in a tetrahedral or truncated tetrahedral coordination resembling that of framework metal atoms:

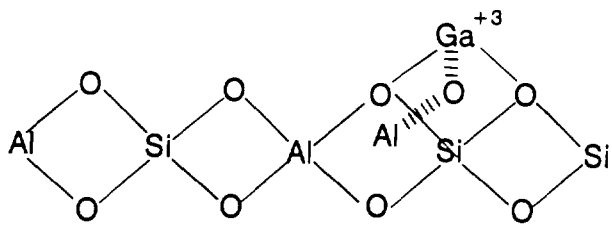

Our proposal also suggests a possible mechanism by which Ga species act as "portholes" (*27*) for the desorption of hydrogen during propane reactions (*10–12*). This step can involve the recombinative desorption of two hydrogens in a GaH_x species or the reaction of hydridic hydrogens on GaH_x with protons from zeolite bridging hydroxyls. In this manner, catalysis proceeds by the continuous decomposition and subsequent reformation of the GaH_x species suggested by our EXAFS studies:

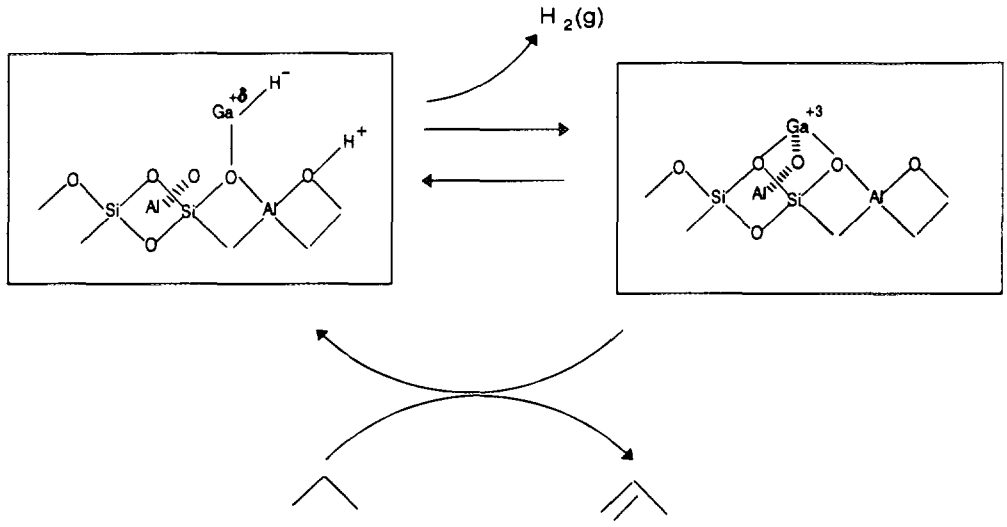

A hydrogen desorption step that requires the cycling of Ga species between reduced and oxidized state is consistent with the heterolytic dissociation of dihydrogen on other oxide surfaces, such as Zn (*32*) and Cr (*39*) oxides. For example, hydrogen chemisorption on ZnO surfaces occurs by the concurrent formation of hydridic and protonic forms of hydrogen adatoms (*32*) and is accompanied by the partial reduction of Zn ions and by the formation of surface hydroxyl groups. The hydrogen recombination step proposed in the above scheme and in Eq. (4) below becomes the microscopic reverse step of this heterolytic hydrogen chemisorption process. We propose that it occurs during alkane dehydrogenation on Ga and Zn ions contained within the channels of H-ZSM5 and other acidic zeolites.

GENESIS OF ACTIVE Ga SPECIES DURING SYNTHESIS AND PRETREATMENT

Impregnation of H-ZSM5 zeolites with Ga nitrate solutions can lead to a mixture of exchanged Ga^{+3}

$$Ga^{+3} + 3NO_3^- \overset{H^+Z^-}{\rightleftharpoons} (Ga^{+3})(Z^-)_3 + 3H^+ + 3NO_3^- \quad (1)$$

and Ga nitrate crystals residing outside zeolite channels,

$$Ga^{+3} + 3NO_3^- \underset{(H^+Z^-)}{\overset{(H^+Z^-)}{\rightleftharpoons}} Ga(NO_3)_3. \quad (2)$$

In the first case, Ga^{+3} cations replace protons in cation-exchange sites within H-ZSM5 channels; this process does not appear to occur readily during the initial impregnation of these samples with Ga nitrate.

During calcination, Ga nitrate crystals decompose to Ga_2O_3, without affecting the density of protons in cation echange sites:

$$2Ga^{3+} + 6NO_3^- \underset{(H^+Z^-)}{\overset{(H^+Z^-)}{\rightleftharpoons}} Ga_2O_3 + 6NO_2 + 3/2\,O_2. \quad (3)$$

In contrast, exchanged Ga^{+3} ions are unaffected by the oxidation treatment, which

only removes HNO_3 residues from zeolite channels. Our near edge measurements show equivalent number of Ga^{+3} species in octahedral and tetrahedral sites, suggesting that calcined materials contain predominantly Ga_2O_3 crystals. Therefore, a majority of the Ga^{+3} species initially reside away from cation exchange sites, where they would exist in tetrahedral-type structures. These data suggest that no significant ion-exchange occurs during the initial impregnation of H-ZSM5 with Ga nitrate.

The previous discussion suggests that exchanged Ga^{+3} ions would decrease zeolite Brønsted acidity by replacing acidic protons in bridging hydroxyls but that extracrystalline Ga_2O_3 species would not. The reactions of 2-methyl-2-pentene, a well-established probe of acid site density and strength (*29, 36*), suggest that Ga^{+3} species formed following calcination of impregnated Ga/H-ZSM5 retain the initial acid site density and strength of the starting H-ZSM5 material (Table 2). The acid site density controls the rate of double-bond (leading to 4-methyl-2-pentene) and methyl (leading to 3-methyl-2-pentene) shift reactions. The ratio of methyl to double-bond shift rates is a measure of acid strength, because methyl-shift carbenium ion reactions require stronger acid sites and longer surface residence times than double-bond migration (*29, 36*). None of these reactive characteristics differ significantly between H-ZSM5 and calcined Ga/H-ZSM5. Moreover, the surface density of strongly adsorbed NH_3 on H-ZSM5 (0.82 NH_3/Al) is almost unchanged by impregnation with Ga nitrate and subsequent calcination (0.77 NH_3/Al) (Table 2). Thus, these catalytic and adsorption studies confirm that Ga^{+3} ions reside predominantly in extracrystalline Ga_2O_3 and not at cation-exchange sites after the initial calcination of Ga/H-ZSM5 materials prepared by impregnation with Ga nitrate.

The reduction of the exchanged Ga^{+3} species, formed by intracrystalline migration at high temperatures, regenerates acidic protons

$$Ga^{+3}(3 \cdot Z^-) + \left(\frac{3-\delta}{2}\right) H_2 \rightleftarrows Ga^{+\delta}(\delta Z^-) + (3-\delta)H^+Z^-, \quad (4)$$

while Ga_2O_3 species reduce instead by removal of oxygen anions as water:

$$Ga_2O_3 + (3-\delta)H_2 + \delta H^+Z^- \rightleftarrows 2Ga^{+\delta}(\delta Z^-) + 3H_2O. \quad (5)$$

In either case, the initial density of acid protons is unchanged following reduction. Indeed, 2-methyl-2-pentene isomerization rates and selectivity on reduced Ga/H-ZSM5 samples are almost identical to those observed on unpromoted H-ZSM5 (Table 2). The reduction process decreases the surface density of strongly adsorbed ammonia (0.82 NH_3/Al on H-ZSM5 to 0.62 NH_3/Al on reduced Ga/H-ZSM5) (Table 2). This observed decrease, the stoichiometry described by Eq.(5), and the ratio of available Ga to cation-exchange sites ($Ga^{+3}/Z^- = 0.28$) lead to an estimate of 1.06 for the value of δ in Eq. (5). It appears that NH_3 adsorption at room temperature also reduces tetrahedral Ga^{+3} species to Ga^{+1} cations interacting with individual (Z^-) exchange sites.

At lower temperatures, even in the presence of gas phase hydrogen, the reverse of reaction (4) becomes favored by thermodynamics and reoxidation of $Ga^{+\delta}$ species by acidic protons occurs. Hydrogen chemisorption uptakes at room temperature (RT) are very low (H/Ga = 0.055) even on Ga/H-ZSM5 samples pretreated in H_2 for 2 h (Fig. 11) before chemisorption experiments. Chemisorption uptakes increase markedly with increasing chemisorption temperature and reach H/Ga values of 0.3–0.4 at 673–773 K, temperatures similar to those required for catalytic reactions of light alkanes on H-ZSM5 and Ga/H-ZSM5. This behavior suggests that the surface density of hydrogen adatoms on Ga/H-ZSM5, formed in dissociative chemisorption steps, becomes significant only at high temperatures (>673 K).

Total chemisorption uptakes on unreduced Ga/H-ZSM5 samples are much lower than on prereduced samples at low chemi-

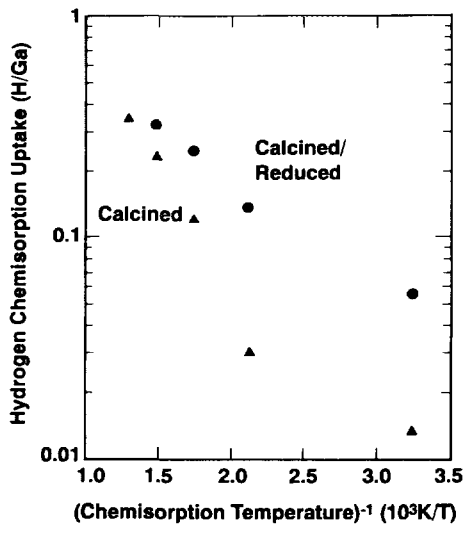

FIG. 11. Temperature dependence of hydrogen chemisorption uptakes on calcined (▲) and calcined–reduced (●) Ga/H-ZSM5 (2.0% wt).

sorption temperatures (Fig. 11). These uptakes increase and approach values similar to those on prereduced samples as the chemisorption temperature increases. The hydrogen consumed during "chemisorption" in the reduction of Ga^{+3} in Ga_2O_3 (Eq. (5)), is not detected in our volumetric adsorption measurements because each H_2 molecule extracted from the gas phase is replaced by a water molecule. This is in contrast to the previously reduced sample, in which volumetric measurements of chemisorption uptakes are not obscured by the release of H_2O. Clearly, chemisorption temperatures near 672–773 K allow the reduction of Ga^{+3} species, less efficiently but in much the same manner as the hydrogen pretreatment of unreduced samples. At high chemisorption temperatures, hydrogen uptakes on reduced and unreduced samples become very similar.

THE ROLE OF Ga IN THE CATALYTIC CONVERSION OF PROPANE ON Ga/H-ZSM5

In this final section, we discuss how the catalytic properties of Ga/H-ZSM5 in reactions of propane to aromatics can be related to the presence of hydridic forms of Ga that exist on the catalyst, but only while the catalytic reactions occur.

The conversion and aromatics selectivity on Ga/H-ZSM5 catalysts increases gradually from values typical of unpromoted H-ZSM5 to steady-state values as propane reactions occur on uncalcined Ga/H-ZSM5 (Table 2). This catalytic behavior parallels the slow formation of hydridic Ga species detected by XAS measurements during the initial reduction treatment. Changes in catalytic behavior occur over 4–8 h, reaction times similar to those required for the attainment of steady-state concentrations of hydridic Ga species. Additional evidence is provided by comparing propane reaction rates and the concentration of GaH_x species in a series of Ga/H-ZSM5 catalysts with varying Ga concentration. Table 2 shows that the rate of propane conversion to aromatics increases as the concentration of hydridic Ga species detected by XAS measurements increases. Increasing concentrations of GaH_x species also lead to a decrease in the cracking selectivity during propane conversion, a feature of the catalytic chemistry caused by a decrease in the surface hydrogen fugacity generated by rate-limiting hydrogen removal steps (*10–12*).

Our proposal may also explain an apparent contradiction between two measurements of the acidity of promoted Ga/H-ZSM5 catalysts. The intensity of infrared hydroxyl bands appears to decrease when Ga is introduced into the channels of H-ZSM5, whether the sample is calcined or reduced before study (*28*). Also, zeolite hydroxyl groups appear to reduce Ga^{+3} with a stoichiometry of two O–H groups per Ga ion (*37*). However, the selectivity of 2-methyl-2-pentene reactions, a sensitive probe of acid site density and strength (*29, 36*), is not strongly influenced by the presence or by the reduction of Ga species in H-ZSM5 (Table 2). Thus, the density of acid sites remains almost unchanged even though Brønsted acid sites associated with bridging (Si–O–Al) hydroxyl groups appear

to decrease as Ga is introduced. If O–GaH_x species replace a fraction of these O–H groups, the resulting stabilized hydride of Ga residing at cation-exchange sites can maintain the Brønsted acidity previously associated with protons in bridging hydroxyl groups. In effect, the ability of the catalytic Ga species to recombine hydridic and protonic hydrogen species to give H_2 is a clear indication that such species provide a stable, but possibly short-lived, binding site for H^- and possibly for H^+ forms of H-adatoms. Clearly, infrared measurements near RT detect only oxidized forms of Ga (Ga^{+3}) residing at cation-exchange sites. Oxidation of GaH_x species near RT and the accompanying desorption of H_2 can indeed decrease the density of bridging O–H groups, as observed in these IR measurements (*28*). These hydroxyl groups and the required Brønsted acidity are restored by the formation of GaH_x species during catalysis at higher temperatures.

Ga species at steady-state provide a "porthole" (*27*) for the exit and entry of hydrogen atoms (from H_2) into catalytic reactions occurring on metal oxide surfaces (*10–12*). The selectivity of propane reactions on H-ZSM5 is not influenced by the pressure of dihydrogen in the contacting gas phase (Fig. 12), because neither dissociative adsorption nor recombinative desorption occur readily during catalysis. In effect, the H-ZSM5 surface is supersaturated with indigenous H-adatoms during propane reactions; these H-adatoms are formed in propane dehydrogenation steps and are present at virtual pressures (*30*) (or surface fugacities (*31*)) significantly exceeding those in the contacting gas phase (*11, 12*). In other words, the hydrogen desorption steps are irreversible and very far from equilibrium; thus, the rate of H_2 adsorption is negligibly small compared with H-adatom desorption rates during propane conversion. In contrast, increasing dihydrogen pressure decreases the aromatics selectivity on Ga/H-ZSM5 to values that begin to approach those on the hydrogen-rich H-ZSM5 surfaces

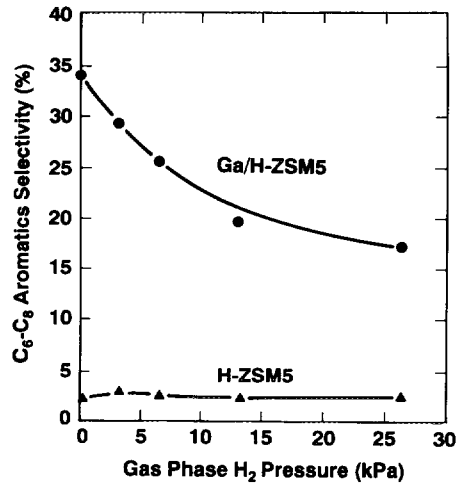

FIG. 12. The effect of dihydrogen pressure on the selectivity of propane dehydrocyclodimerization on H-ZSM5 and Ga/H-ZSM5 [steady-state prereduced catalyst; 773 K, 26.6 kPa propane, balance He, 8–12% propane conversion].

(Fig. 12). The presence of Ga species permits reversible communication between surface and gas phase (H_2) pools of H-atoms, a proposal consistent with deuterium exchange measurements reported previously (*10–12*). Similar observations on Zn/H-ZSM5 catalysts were also attributed to a hydrogen desorption rate-limiting step that was partially relieved by the presence of Zn species within H-ZSM5 channels (*5, 12*).

The recombinative desorption of hydrogen adatoms as H_2 becomes increasingly responsible for the removal of hydrogen adatoms during propane conversion when Ga or Zn species are introduced into H-ZSM5 catalysts (Fig. 13). The fraction of the hydrogen in converted propane that is removed as H_2 is much higher on samples containing Ga and Zn than on unpromoted H-ZSM5 (Fig. 13). Recombinative desorption replaces hydrogen transfer to surface intermediates and required cracking of adsorbed hydrocarbons as the predominant hydrogen removal mechanisms during propane conversion to aromatics. As a result, cracking selectivity decreases markedly

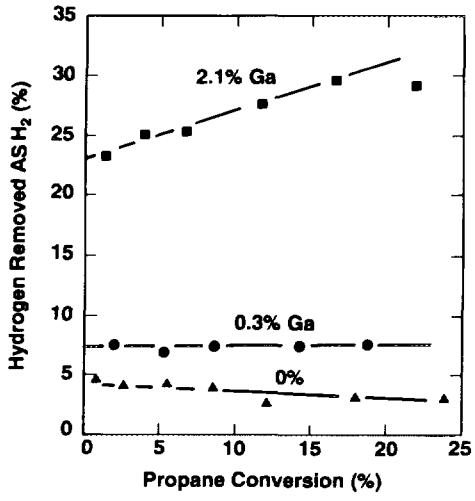

FIG. 13. Hydrogen removed as H_2 during reactions of propane on H-ZSM5 and Ga/H-ZSM5, [steady-state prereduced catalysts; 773 K, 26.6 kPa propane, balance He].

when H-ZSM5 catalysts are promoted with either Ga or Zn.

THE ROLE OF Zn IONS IN CATALYTIC REACTIONS OF PROPANE

Zn ions also increase the rate and aromatics selectivity in propane reactions on H-ZSM5 (*5*, *12*). *In-situ* XAS studies of Zn/H-ZSM5 catalysts show that Zn^{+2} ions do not reduce significantly during H_2 pretreatment or propane reactions at 773 K. Also, these materials did not require a H_2 pretreatment or extensive activation during catalysis in order to achieve steady-state catalytic rates and selectivities.

In-situ XAS studies, however, detected a clear change in the Zn^{+2} coordination sphere, reflected in both the near-edge and the EXAFS energy regions. These changes may reflect the disruption of Zn–O bonds in near surface regions by the heterolytic chemisorption of hydrogen during pretreatment and propane reactions. These results will be described and discussed in detail elsewhere (*40*).

Dent and Kokes (*32*) have previously shown that H_2 dissociates heterolytically on Zn–O pairs during ethylene hydrogenation reaction on zinc oxide. The reverse of this process may also account for the ability of zinc oxide to catalyze the desorption of H-adatoms (H^+ and H^-), in much the same manner as we have proposed for catalytic hydrogen desorption on Ga species within H-ZSM5 (*11*, *12*).

CONCLUSIONS

Ga^{+3} species initially present in calcined Ga/H-ZSM5 materials reduce during hydrogen pretreatment or propane dehydrocyclodimerization reactions. Propane conversion turnover rates, aromatics selectivity, and the ability to remove hydrogen as H_2 (and not as cracking products) also increase as reduction occurs. This reduced form of Ga (GaH_x, $+\delta$ oxidation state) resembles zero-valent Ga in the energy of the X-ray absorption edge but lacks the fine structure expected of Ga metal. The weak EXAFS features suggest that reduced Ga species lose significant coordination to oxygen during reduction; they appear to change from bulk oxide-like structure into isolated $Ga^{+\delta}$ atoms in oxidation states between 0 and 1 coordinated to the equivalent of a single basic oxygen within zeolite channels.

We propose that such monomeric $Ga^{+\delta}$ species probably occur in the form of hydride compounds of Ga stabilized by coordination to basic oxygens. This is consistent with the decomposition and self-oxidation to tetrahedral Ga^{+3} that occur when reduced samples are cooled to RT in a hydrogen or inert atmosphere. Therefore, the catalytic Ga species is unstable near RT; it is detectable only at reaction conditions in the presence of a reducing agent such as H_2 or propane. These catalytic sites can not be detected by analysis of Ga/H-ZSM5 catalysts before and after propane reactions; these characterization protocols would incorrectly conclude that tetrahedral (framework) Ga^{+3} ions account for the active hydrogen desorption sites introduced by Ga.

The proposed ligand-stabilized Ga hydride is certainly unstable with respect to

recombinative and oxidative loss of hydrogen and must be replenished continuously by a kinetic process that forms H-adatoms. The catalytic behavior of these hydrides requires that reactions be carried out near the limit of their thermal stability in order to ensure their rapid decomposition and reformation, processes that lead to the net desorption of H_2 during alkane dehydrogenation reactions. Hydrides of other metals may also become sufficiently stable by ligand stabilization near the temperatures required to cause the cleavage of C–H bonds in alkanes. Thus, we expect that metallic or oxidic forms of these elements will also yield useful dehydrogenation functions when introduced on the surface of non-reducible metal oxides (such as $SiO_2 \cdot Al_2O_3$); these nonreducible oxides can activate C–H bonds but are unable to desorb the resulting H-adatoms as H_2. In these cases, as in the case of Ga/H-ZSM5, the limited stability and the facile re-oxidation of active stabilized hydrides will require that we detect them by *in-situ* structural characterization at the conditions required for the catalytic reactions to occur.

ACKNOWLEDGMENTS

We thank Dr. G. B. McVicker and Mr. J. J. Ziemiak for the 2-methyl-2-pentene acidity characterization, Mr. C. J. McCoy for the chemisorption measurements, and Dr. S. C. Fung for the temperature-programmed reduction measurements. We also thank Dr. D. E. W. Vaughan and Mr. Karl Strohmeier for the standard gallosilicate sample, and Mr. Gregory DeMartin and Dr. Stuart Soled for the ammonia adsorption measurements.

REFERENCES

1. Gregory, R., and Kolombos, A. J., U.S. Patent 4 056 575 (1977).
2. Bulford, S. N., and Davies, E. E., U.S. Patent 4 157 356 (1979).
3. Kitagawa, H., Sendoda, Y., and Ono, Y., *J. Catal.* **101,** 12 (1986).
4. Mowry, J. R., Anderson, R. F., and Johnson, J. A., *Oil Gas J.* **83,** 1288 (1985).
5. Mole, T., Anderson, J. R., and Creer, G., *Appl. Catal.* **17,** 141 (1985).
6. Meriadeau, P., and Naccache, C., *J. Mol. Catal.* **59,** L31 (1990).
7. Yao, J., le van Mao, R., and Dufresne, L., *Appl. Catal.* **65,** 175 (1990).
8. Fujimoto, K., Nakamura, I., Yokota, K., and Aimoto, K., *Bull. Chem. Soc. Jpn.* **64,** 2275 (1991).
9. Okabe, K., Matsubayashi, N., Sayama, K., Arakawa, H., and Nishijima, A., *Bull. Chem. Soc. Jpn.* **64,** 2602 (1991).
10. Iglesia, E., and Baumgartner, J. E., *in* "Abstr. Proc. 12th North American Meeting of the Catalysis Society, Lexington, KY, 1991."
11. Iglesia, E., Baumgartner, J. E., and Price, G. L., *J. Catal.* **134,** 549 (1992).
12. Iglesia, E., Baumgartner, J. E., and Meitzner, G. D., *in* "Proceedings, 10th International Congress on Catalysis" (Guczi, L. Ed.), in press.
13. Iglesia, E., Baumgartner, J. E., Price, G. L., Rose, K. D., and Robbins, J. L., *J. Catal.* **125,** 95 (1990).
14. Axon, S. A., Huddersman, K., and Klinowski, J., *Chem. Phys. Lett.* **172,** 398 (1990); Lalik, E., Liu, X., and Klinowski, J., *J. Phys. Chem.* **96,** 805 (1992).
15. Bayense, C. R., Kentgens, A. P. M., deHaan, J. W., van de Ven, L. J. M., and van Hooff, J. H. C., *J. Phys. Chem.* **96,** 775 (1992).
16. Axon, S. A., Barrie, P. J., Fox, K. K., Carr, S. W., and Klinowski, J., *Mat. Res. Soc. Ext. Abstr.* **EA-24** (1990).
17. Sansone, M., Via, G. H., George, G., Meitzner, G. D., and Hewitt, R., *in* "X-Ray Absorption Fine Structure," (S. S. Hasnain, Ed.), p. 656, Ellis–Norwood, New York, 1991.
18. Meitzner, G. D., and Huang, E. S., *Fresenius' J. Anal. Chem.* **342,** 61 (1992).
19. Vaughan, D. E. W., and Strohmeier, K., Ludox and sodium gallate synthesis, using TPA and TBA templates, personal communication.
20. Lytle, F. W., Wei, P. S. P., Greegor, R. B., Via, G. H., and Sinfelt, J. H., *J. Chem. Phys.* **70,** 4849 (1979).
21. Cramer, S. P., Eccles, T. K., Kutzler, F. W., Hodgson, K. O., and Mortenson, L. E., *J. Am. Chem. Soc.* **98,** 1287 (1976).
22. McKale, A. G., Veal, B. W., Paulikas, A. P., Chan, S.-K., and Knapp, G. S., *Solid State Commun.* **29,** 481 (1979).
23. Timken, H.-K. C., and Oldfield, E., *J. Am. Chem. Soc.* **109,** 7669 (1987).
24. Wade, K., and Banister, A. J., *in* "Comprehensive Inorganic Chemistry" (J. C. Bailer, H. J. Emeleus, R. Hyholm, and A. F. Trotman-Dickenson, Eds.), Vol. 1, pp. 993–1064. Pergamon Press, New York, 1973.
25. Reed, T. B., "Free Energy of Formation of Binary Compounds: An Atlas of Charts for High-Temperature Chemical Calculations." MIT Press, Cambridge, MA, 1971.

26. Wade, K., and Banister, A. J., *in* "Comprehensive Inorganic Chemistry," (J. C. Bailer, H. J. Emeleus, R. Hyholm, and A. F. Trotman-Dickenson, Eds.), Vol. 1, pp. 1065–1117.
27. Taylor, H. S., *Annu. Rev. Phys. Chem.* **12,** 127 (1961).
28. Meriaudeau, P., and Naccache, C., *Appl. Catal.* **73,** L13 (1991).
29. Kramer, G. M., and McVicker, G. B., *Acc. Chem. Res.* **19,** 78 (1986).
30. Temkin, M. I., and Pyzhev, V., *Acta Physicochim.* **12,** 327 (1940).
31. Boudart, M., *Ind. Eng. Chem. Fundam.* **25,** 70 (1986).
32. Dent, A. L., and Kokes, R. J., *J. Phys. Chem.* **73** (1969) 3772; Kokes, R. J., and Dent, A. L., *in* "Advances in Catalysis and Related Subjects" (D. D. Eley, H. Pines, and P. B. Weisz, Eds.), Vol. 22, p. 1. Academic Press, New York, 1972.
33. Eisenberger, P. M., and Brown, G. S., *Solid State Commun.* **29,** 481 (1979).
34. Price, G. L., and Kanazierev, V., *J. Catal.* **126,** 267 (1990); *J. Mol. Catal.* **66,** 115 (1991).
35. Zhang, Z., Xu, L., and Sachtler, W. M. H., *J. Catal.* **131,** 502 (1991).
36. Kramer, G. M., McVicker, G. B., and Ziemiak, J. J., *J. Catal.* **92,** 335 (1985).
37. Kanazirev, V., Dimitrova, R., Price, G. L., Khodakov, A. Yu., Kustov, M., and Kazansky, V. B., *J. Mol. Catal.* **70,** 111 (1991).
38. Shriver, D. F., and Nordman, C. E., *Inorg. Chem.* **2,** 1298 (1963).
39. Burwell, R. L., Jr., and Stec, K. S., *J. Colloid Interface Sci.* **58,** 54 (1977); Burwell, R. L., Jr., Haller, G. L., Taylor, K. C., and Read, J. F., *in* "Advances in Catalysis and Related Subjects" (D. D. Eley, H. Pines, and P. B. Weisz, Eds.), Vol. 20, p. 1. Academic Press, New York, 1970.
40. Meitzner, G. D., Iglesia, E., and Baumgartner, J. E., *J. Catal.*, submitted.
41. Fung, S. C., Meitzner, G. D., Baumgartner, J. E., and Iglesia, E., *J. Catal.*, submitted.